

SBA-15 as a Support for Nickel-Based Catalysts for Polymerization Reactions

Anderson J. Schwanke,^a Cristiano Favero,^b Rosana Balzer,^c Katia Bernardo-Gusmão^b
and Sibe B. C. Pergher^{*a}

^aPrograma de Pós-Graduação em Ciência e Engenharia de Materiais, Instituto de Química,
Universidade Federal do Rio Grande do Norte (UFRN), 59078-970 Natal-RN, Brazil

^bInstituto de Química, Universidade Federal do Rio Grande do Sul (UFRGS),
91501-970 Porto Alegre-RS, Brazil

^cDepartamento de Engenharias e Exatas, Universidade Federal do Paraná (UFPR),
85950-000 Palotina-PR, Brazil

Two mesoporous SBA-15 materials with different morphologies (spherical and fiber-shaped) were synthesized and evaluated as supports for nickel-based catalysts for polymerization reactions. The supports were pretreated with trimethylaluminum (TMA), and the catalyst dibromo-bis(4-amino-2,3,5,6-tetramethylimino)acenaphthene nickel(II) was attached to the supports and activated with TMA or MAO (methylaluminoxane). Characterization showed that the insertion of cetyltrimethylammonium bromide (CTABr) as a cosurfactant led to spherical SBA-15 with a decrease in particle and pore sizes to 4.8 nm compared to 6.5 nm in traditional fiber-shaped SBA-15. The spherical SBA-15 showed thicker walls than the fiber-shaped SBA-15, attributed to the increase in functional groups of the cosurfactant. The different spherical and fiber-shaped morphologies did not show any significant difference in the productivity of polyethylene. The catalyst supported on spherical SBA-15 materials showed 58% productivity compared to its homogeneous analogue using TMA as a cocatalyst.

Keywords: SBA-15, mesoporous, morphological control, polymerization

Introduction

The transition metal-catalyzed olefin polymerization reaction is very important in the chemical industry.¹ Therefore, the nickel-based catalysts obtained by Brookhart and co-workers² have been intensively studied. These catalysts have high catalytic activity and represent a pathway for traditional systems to polymerize polar monomers, obtaining control of the microstructure and promoting chain branching without the use of other monomers. However, polymerization in a homogeneous medium has the drawback of using a large volume of solvents and large reactors in which efficient control of temperature is required.³

Mesoporous silica materials have attracted great attention since their discovery in 1992.^{4,5} Among this class of materials, SBA-15 mesoporous silica has controllable large mesopore sizes (5-15 nm) with a narrow pore size

distribution and high surface area (> 500 m² g⁻¹) and thick pore walls, leading to good stability. Therefore, SBA-15 materials have been applied in many fields, including catalysis, adsorption, separation, medicine and enzyme immobilization.⁶⁻¹⁰

The control of its structural properties relies on the synthesis conditions, e.g., temperature, stirring, micelle packaging parameters and the addition of cosurfactants and solvents. These modifications can lead to SBA-15 mesoporous material with different type-morphologies, including spheres, platelets, nanorods, rice shapes and hexagonal columns.^{11,12} Specifically, the application of mesoporous materials with spherical-shaped particles has been reported as drug delivery systems, the stationary phase in high-performance liquid chromatography (HPLC) columns and, recently, supports to metals in nickel and molybdenum-based catalysts.¹³⁻¹⁵ For all these applications, the spherical morphology showed higher performance than traditional fiber-shaped SBA-15 due to improved diffusion to the reactants or dispersion of the active centers.

*e-mail: sibepergher@gmail.com

Other porous materials were used as supports for the polymerization of olefins, e.g., layered double hydroxides, silica-zirconia and silica-alumina supports and chrysotile.¹⁶⁻¹⁸ Mesoporous materials (MCM-41 and SBA-15) have previously been used as catalyst supports.^{19,20} However, studies comparing the influence of different morphologies of the supports are infrequent. Here, we discuss the synthesis of spherical and fiber SBA-15 as supports for nickel-based catalysts for olefin polymerization and discuss parameters including the Al/Ni ratio, volume of solvent, temperature and the aluminum activator.

Experimental

Synthesis of spherical and traditional fiber-shaped SBA-15 supports

The synthesis of spherical SBA-15 (sSBA-15) was performed using 2.0 g Pluronic P123 (tri-block copolymer poly(ethylene oxide)-poly(propylene oxide)-poly(ethylene oxide)) and 0.2 g cetyltrimethylammonium bromide (CTABr, 99%) dissolved in a mixture of 45.0 g deionized water, 30.0 g HCl (2 mol L⁻¹) and 5.8 g tetraethyl orthosilicate (TEOS, 98%). The mixture was stirred at 300 rpm for 20 h at 40 °C. The gel was transferred into a Teflon bottle and heated at 100 °C for 24 h. The solid was filtered and dried at room temperature. The synthesis of traditional fiber-shaped SBA-15 (tSBA-15) was performed under the same conditions without the addition of CTABr. All reagents used were from Sigma-Aldrich. The samples were calcined (c) in nitrogen (gas flow 1 cm³ s⁻¹) at 540 °C (heating rate of 3 °C min⁻¹). After reaching the temperature, nitrogen was replaced by synthetic air (gas flow 1 cm³ s⁻¹) for 8 h at 540 °C. The nitrogen and synthetic air used were from White Martins (grade 5.0).

Pretreatment of the supports

Within a suspension of the sSBA-15c or tSBA-15c (1.4 g in 10.0 mL dry toluene, distilled over metallic sodium), 20 mL of a TMA solution in toluene (1.5 mmol mL⁻¹) was added. The reaction proceeded under magnetic stirring

for 18 h. The solid was removed by filtration under an inert atmosphere (argon) and washed consecutively with five aliquots of 15 mL toluene. The pretreated sSBA-15c and tSBA-15c were dried under reduced pressure and subsequently used for the immobilization of the catalytic precursor.

Synthesis of the catalyst precursor

The ligand was synthesized by the condensation reaction between acenaphthoquinone and 2,3,5,6-tetramethyl-*p*-phenylenediamine, catalyzed by sulfuric acid.²¹ Then, the catalyst precursor was obtained by complexation of the ligand with a metal adduct of nickel(II) bromide and acetonitrile (Ni(MeCN)₂Br₂) under argon atmosphere. Acetonitrile and dichloromethane were dried and distilled over P₂O₅ and stored under argon. The complexation reaction occurred at room temperature for 72 h in dichloromethane, as shown in Figure 1, for the formation of the homogeneous catalyst precursor dibromo-bis(4-amino-2,3,5,6-tetramethylimino)acenaphthene nickel(II), named C1.

Immobilization of C1 on the pretreated supports

The precursor was immobilized by adding 10 mL of a solution of 6.7 μmol mL⁻¹ of C1 in dichloromethane to a suspension containing 1.32 g of the pretreated sSBA-15c or tSBA-15c in 10 mL dichloromethane. The immobilization reaction was performed at room temperature for 18 h. The original black solution turned into a clear solution after the reaction. The solvent was removed after completing the reaction, and the catalyst was directly used for the polymerization reactions. The nickel content sSBA-15c-C1 and tSBA-15c-C1 was determined by atomic absorption spectroscopy (AAS) with 96.7 and 97.5% of the original catalyst load (67.4 μmol) anchored on the support, respectively.

Polymerization reactions

The polymerization reaction was carried out in a 200 mL glass jacketed reactor with a thermostatic circulation bath

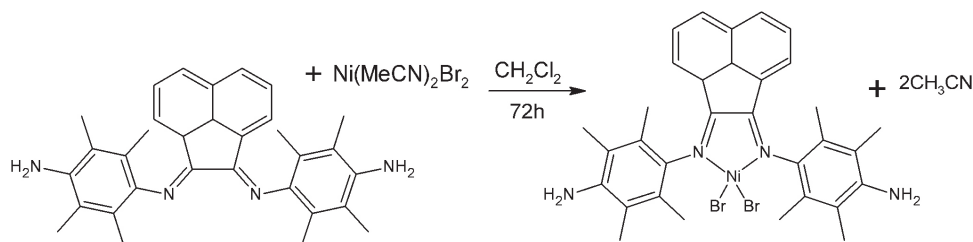


Figure 1. Synthesis of catalytic precursor dibromo-bis(4-amino-2,3,5,6-tetramethylimino)acenaphthene nickel(II), named C1.

with controlled temperature. During the experiment, the reaction was homogenized by magnetic stirring. Dry toluene was used as the solvent and added to the reactor with a syringe under argon flow. The cocatalyst was added and stirred for five minutes. The system was purged five times with ethylene and saturated for five minutes. Finally, the precursor solution or the suspension of the heterogenized catalyst was added to the reactor after depressurization. The reaction started upon adding the precatalyst, kept under a continuous flow of ethylene at 4 bar. At the desired time, the polymer was precipitated in acidified ethanol (5% HCl), washed consecutively with water and ethanol, filtered and dried under reduced pressure.

Characterization

Small-angle X-ray powder diffraction (XRD) was performed on a Bruker diffractometer, model D2 Phaser, with a Ni filter, CuK α radiation ($\lambda = 1.54 \text{ \AA}$), and a voltage of 30 kV using a Lynxeye detector. The scanning was performed at 2θ angles from 0.7 to 4.0° . The nitrogen adsorption and desorption isotherms at $-196 \text{ }^\circ\text{C}$ were obtained using a Micrometrics Tristar II (model 3020). The samples were pretreated under vacuum (10^{-1} bar) at $300 \text{ }^\circ\text{C}$ for 10 h. The surface area of the samples was calculated by the BET (Brunauer-Emmett-Teller) equation,²² using relative pressure regions $p/p^0 = 0.05$ to 0.20 . The pore size distribution was calculated using the BJH (Barrett-Joyner-Halenda) method.²³ Scanning electronic microscopy (SEM) analyses were performed

using a Carl Zeiss scanning electron microscope model EVO50 operating in the variable pressure mode with an accelerating voltage of 5 kV and a secondary electron detector. Transmission electron microscopy (TEM) analyses were performed using a Philips (model CM10) with an operating voltage of 100 kV. Atomic absorption spectroscopy (AAS) analyses were performed using a PerkinElmer A model Analyst 200. The polymers were characterized by differential scanning calorimetry (DSC) in a TA Instruments model Q20/RCS40 with cycles of heating and cooling. A small sample of polyethylene (5-10 mg) was heated and cooled at $10 \text{ }^\circ\text{C min}^{-1}$ over temperatures ranging from 30 to $180 \text{ }^\circ\text{C}$. Two cycles were performed, and the second cycle was used in our calculations for the crystallinity (χ_c) and melting point (T_m).

Results and Discussion

The small-angle XRD and nitrogen adsorption and desorption isotherms of spherical and traditional fiber-shaped SBA-15 materials are shown in Figure 2. In general, the XRD patterns characteristic of long-range ordering are observed for both samples after calcination. The three diffraction bands are characteristic of planes 100, 110 and 200 with hexagonal symmetry.²⁴

The XRD patterns of as-synthesized traditional fiber-shaped SBA-15 showed a contraction of 0.8 nm after calcination. This contraction is attributed to structural rearrangements by dehydration, dehydroxylation and the

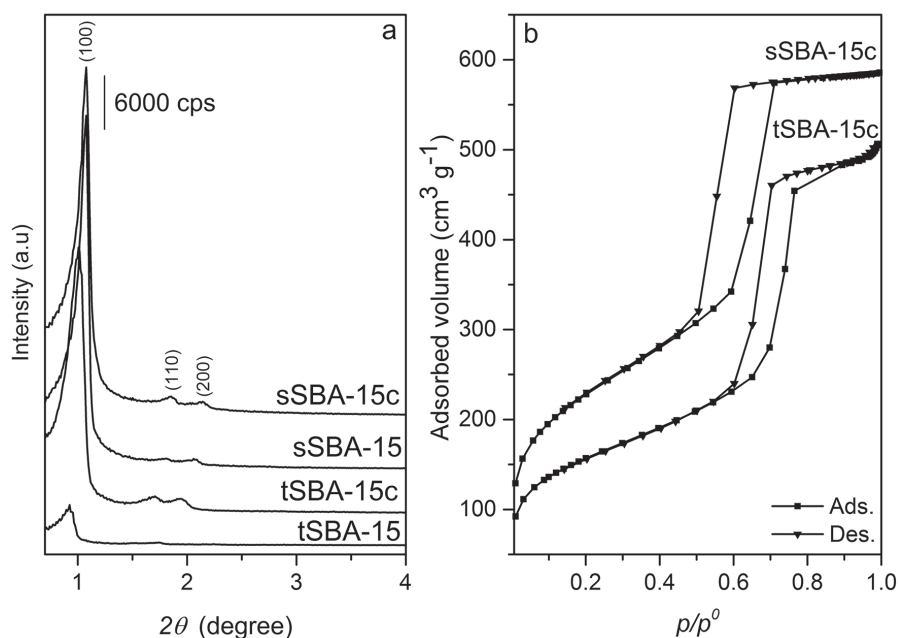


Figure 2. Small-angle XRD of as-synthesized and calcined spherical and traditional fiber-shaped SBA-15 (a) and nitrogen adsorption and desorption isotherms of calcined samples (b).

Table 1. Textural properties of traditional and spherical SBA-15 calcined materials

Sample	d_{100} / nm	a_0 / nm	S_{BET} / ($\text{m}^2 \text{g}^{-1}$)	S_{micro} / ($\text{m}^2 \text{g}^{-1}$)	S_{ext} / ($\text{m}^2 \text{g}^{-1}$)	V_{micro} / ($\text{cm}^3 \text{g}^{-1}$)	V_{meso} / ($\text{cm}^3 \text{g}^{-1}$)	D_p / nm	W_t / nm
sSBA-15c	8.7	10.1	819	134	685	0.05	0.9	4.8	5.3
tSBA-15c	8.8	10.2	558	101	457	0.04	0.8	6.5	3.7

a_0 : lattice parameters = $2d_{100}/\sqrt{3}$; S_{BET} : BET surface area; S_{micro} : microporous surface area; S_{ext} : external surface area; V_{micro} : microporous volume; V_{meso} : mesoporous volume; D_p : pore diameter; W_t : wall thickness = $a_0 - D_p$.

formation of siloxane bonds, producing a silica with a more condensed structure.²⁵ However, this contraction did not occur for as-synthesized and calcined spherical SBA-15 samples.

The nitrogen adsorption and desorption isotherms for spherical and traditional fiber-shaped SBA-15 are shown in Figure 2b. Both calcined materials showed type IVa isotherms, characteristic of mesoporous materials, according to IUPAC.²⁶ The abrupt increase in the adsorbed amount of nitrogen at p/p^0 ranging from 0.6 to 0.8 corresponds to the region of capillary condensation within the uniform mesopores. Both SBA-15 samples exhibit type H1 hysteresis with irreversible cycles related to the geometry of well-ordered open cylindrical pores.²⁶ The pore diameter showed values centered at 4.8 and 6.5 nm for the spherical and traditional fiber-shaped SBA-15 materials, respectively.

Table 1 shows the textural properties of spherical and traditional fiber-shaped SBA-15. The spherical SBA-15 showed a surface area (S_{BET}) of $819 \text{ m}^2 \text{g}^{-1}$, and the traditional fiber-shaped SBA-15 showed $558 \text{ m}^2 \text{g}^{-1}$. Both samples have similar values of the microporous surface area (S_{micro}), which interconnects the mesoporous channels.

It was observed that the lattice parameters (a_0) for spherical and traditional fiber-shaped SBA-15 samples are similar. However, the pore diameter of spherical SBA-15 is 1.7 nm smaller than for traditional fiber-shaped SBA-15. We attributed this to the increase in functional groups (provided by cosurfactant, CTABr) with nonionic P123 copolymer, attracting more silica species and producing a material with an increased wall thickness. Indeed, similar behavior was reported by Ryoo and co-workers²⁷ for the synthesis of mesoporous silica. The increased wall thickness (W_t) for spherical SBA-15 increases the stability of the material. On the other hand, the decrease in pore diameter could limit the access of the catalytic precursor.

SEM images of spherical and traditional fiber-shaped SBA-15 materials are shown in Figure 3. Homogeneous spheres were observed with sizes ranging from 0.5 to $2.5 \mu\text{m}$ (images a and b), clearly different from traditional fiber-shaped SBA-15 (images c and d). The synthesis of SBA-15 with the single copolymer P123 leads to a

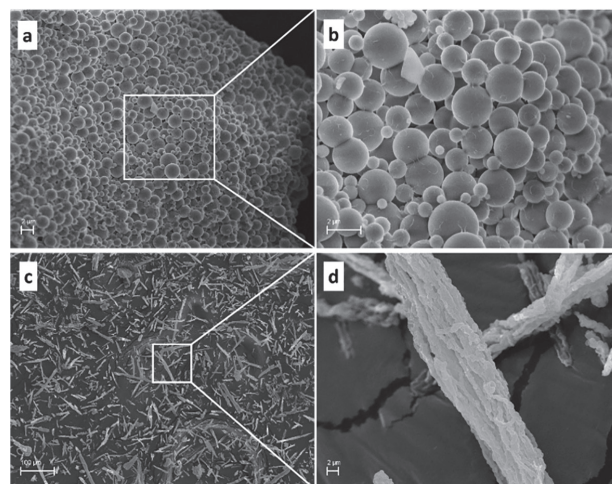


Figure 3. SEM of spherical sSBA-15c with magnifications of (a) 5,000 \times and (b) 15,000 \times . Images of traditional tSBA-15c with magnifications of (c) 300 \times and (d) 5,000 \times .

fiber-shaped morphology of the agglomerated particles with lengths and widths ranging between $80\text{--}100 \mu\text{m}$ and $3\text{--}9 \mu\text{m}$, respectively.

The TEM analyses of spherical and traditional fiber-shaped SBA-15 materials are shown in Figure 4, and the hexagonal honeycomb pore structure was observed for both samples. In addition, the measurements of pore size and pore walls are in good agreement with the related XRD and nitrogen adsorption results. Figure 5 summarized the proposed assembly of single P123 and mixed P123-CTABr

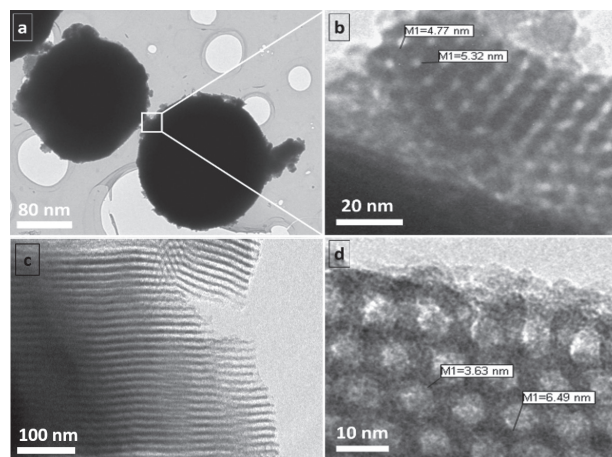


Figure 4. TEM of spherical sSBA-15c (a, b) and traditional fiber-shaped tSBA-15 (c, d).

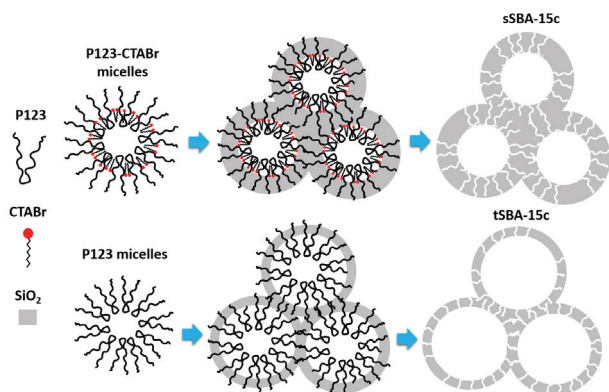


Figure 5. Proposed assembly of single P123 or mixed P123-CTABr micelles and the final spherical and traditional SBA-15 mesoporous structure.

micelles for the formation of the final SBA-15 mesoporous structure.

The spherical and traditional fiber-shaped SBA-15 materials were used as supports for heterogenization of the catalyst precursor C1, and the results of the polymerization reactions are shown in Table 2. In general, the precursor C1 was heterogenized on the spherical (entry 5) and traditional fiber-shaped (entry 4) SBA-15 with a partial decrease in catalytic activity compared to the homogeneous precursor C1 (entry 1). The sSBA-15c-C1 showed 72% of the homogeneous productivity, and tSBA-15-C1 showed 74%, indicating that both the supports and the methodology of heterogenization were appropriate. Due to the morphological differences between spherical and traditional fiber-shaped SBA-15, the pore diameter sSBA-15c is 1.7 nm smaller than in tSBA-15c. On the other hand, the surface area of sSBA-15c

is higher ($261 \text{ m}^2 \text{ g}^{-1}$) than tSBA-15c, which is related to the smaller particle size of sSBA-15c, which resulted in shorter channels. Thus, shorter channels may allow access of the monomer and cocatalyst to the active centers and compensate for the small pore sizes of sSBA-15c, giving similar results in terms of polyethylene productivity.

Due to this similarity, other reaction conditions were used with spherical SBA-15c-C1 and are reported in entries 5 to 12. One benefit related to the use of the heterogenized catalysts is their applicability in more advantageous processes such as gas phase or slurry polymerization.²¹ Therefore, the solvent volume used in each experiment was evaluated (entries 5 and 6). The results showed that even in more concentrated or diluted experiments, the catalytic activity remained constant. In addition, the crystallinity was also constant, which demonstrates that the heterogenized precursor could be used for other processes with a smaller volume of solvent without a decrease in catalytic activity. The effect of the activator (MAO or TMA) is shown in entries 7-8 and 9-10. For the reaction system, TMA proved to be a better activator at lower temperatures ($30 \text{ }^\circ\text{C}$), while MAO was better at $60 \text{ }^\circ\text{C}$. In addition, polymers with higher crystallinity were produced using TMA than MAO.

Entries 6 and 7 show an increase of productivity with decreasing reaction time, where the catalyst is more active in the first minutes. On the other hand, increasing the temperature of the reaction (entries 5, 9 and 10) led to a decrease in the polymerization rate, with a drop in activity for the homogeneous and heterogeneous systems and for both cocatalysts. Similar behavior has been reported in the literature.²⁸ The Al/Ni ratio for both catalysts was also

Table 2. Results of the polymerization reaction with both heterogenized SBA-15c-C1 and homogeneous nickel-based catalyst C1

System	entry	time / min	T / $^\circ\text{C}$	Cocatalyst	Al/Ni	Solvent / mL	PE / g	Productivity / (kg PE mol Ni ⁻¹ h ⁻¹)	χ_c / %	Tm / $^\circ\text{C}$
Homogeneous C1	1	30	30	MAO	325	60	3.7	2437	14	125
	2	10	30	TMA	325	30	2.3	4510	18	125
	3	10	60	TMA	325	30	0.4	960	NF	NF
tSBA-15c-C1	4	30	30	MAO	325	60	2.8	1811	33	120
	5	30	30	MAO	325	60	2.7	1751	28	121
	6	30	30	MAO	325	30	2.5	1641	29	122
sSBA-15c-C1	7	10	30	MAO	325	30	0.9	1858	28	120
	8	10	30	TMA	325	30	1.3	2613	38	129
	9	10	60	TMA	325	30	0.3	722	11	122
	10	10	60	MAO	325	30	0.4	936	7	116
	11	10	30	TMA	55	30	0.5	1084	31	128
	12	10	30	MAO	55	30	0.3	641	37	122

Reaction conditions: 200 mL reactor with control of temperature and stirring. Ethylene pressure 4 bar, MAO or TMA solution and $3.1 \mu\text{mol}$ of catalytic precursor. PE: polyethylene; χ_c : crystallinity; Tm: melting point; NF: not found.

varied (entries 11 and 12), and the results showed that even at very low Al/Ni ratios, moderate activity was achieved. Two distinct melting points were found for entry 11, suggesting a bimodal distribution of the polymeric chains under these conditions.

The catalyst precursor C1 supported on spherical SBA-15 showed 58% activity compared to the homogeneous catalyst at 30 °C (entries 2 and 8) and similar activity at higher temperatures (entries 3, 9 and 10). The system showed better performance with TMA as cocatalyst than MAO (entries 7 and 8).

Conclusions

Two mesoporous SBA-15 silica materials with different morphologies were synthesized. The use of CTABr as a cosurfactant produced spherical SBA-15 with smaller particles and pore sizes than traditional fiber-shaped SBA-15. Both SBA-15 supports were efficient catalytic supports for a nickel-based catalyst precursor, with similar activity. The activity for the catalyst supported on spherical SBA-15 was 72% for 30 min of reaction and 58% for 10 min of reaction compared with the homogeneous analogue. Under different reaction conditions, the supported catalysts exhibit more stable active centers, enhancing the catalytic activity. The precursor was active under adverse conditions such as less solvent and lower Al/Ni ratios.

Acknowledgments

The authors acknowledge the support provided by UFRN, UFRGS and CNPq.

References

- Coates, G. W.; Waymouth, R. M.; *Science* **1995**, *267*, 217.
- Johnson, L. K.; Killian, C. M.; Brookhart, M.; *J. Am. Chem. Soc.* **1995**, *117*, 6414.
- Severn, J. R.; Chadwick, J. C.; Duchateau, R.; Friederichs, N.; *Chem. Rev.* **2005**, *105*, 4073.
- Kresge, C. T.; Leonowicz, M. E.; Roth, W. J.; Vartuli, J. C.; Beck, J. S.; *Nature* **1992**, *359*, 710.
- Beck, J. S.; Vartuli, J. C.; Roth, W. J.; Leonowicz, M. E.; Kresge, C. T.; Schmitt, K. D.; Chu, C. T. W.; Olson, D. H.; Sheppard, E. W.; *J. Am. Chem. Soc.* **1992**, *114*, 10834.
- Zhao, D.; Feng, J.; Huo, Q.; Melosh, N.; Fredrickson, G. H.; Chmelka, B. F.; Stucky, G. D.; *Science* **1998**, *279*, 548.
- Zhou, L.; Fan, J.; Cui, G.; Shang, X.; Tang, Q.; Wang, J.; Fan, M.; *Green Chem.* **2014**, *16*, 4009.
- Timm, J.; Stoltenberg, C.; Senker, J.; Bensch, W.; *Z. Anorg. Allg. Chem.* **2014**, *640*, 595.
- Bahrami, Z.; Badiei, A.; Atyabi, F.; *Chem. Eng. Res. Des.* **2014**, *92*, 1296.
- Yiu, H. H. P.; Wright, P. A.; Botting, N. P.; *J. Mol. Catal. B: Enzym.* **2001**, *15*, 81.
- Lee, H. I.; Kim, J. H.; Stucky, G. D.; Shi, Y.; Pak, C.; Kim, J. M.; *J. Mater. Chem. A* **2010**, *20*, 8483.
- Zhao, D.; Sun, J.; Li, Q.; Stucky, G. D.; *Chem. Mater.* **2000**, *12*, 275.
- Lai, C.-Y.; Trewyn, B. G.; Jeftinija, D. M.; Jeftinija, K.; Xu, S.; Jeftinija, S.; Lin, V. S. Y.; *J. Am. Chem. Soc.* **2003**, *125*, 4451.
- Yasmin, T.; Müller, K.; *J. Chromatogr. A* **2011**, *1218*, 6464.
- Gao, D.; Duan, A.; Zhang, X.; Zhao, Z.; E, H.; Li, J.; Wang, H.; *Appl. Catal., B* **2015**, *165*, 269.
- Buffet, J.-C.; Wanna, N.; Arnold, T. A. Q.; Gibson, E. K.; Wells, P. P.; Wang, Q.; Tantirungrotechai, J.; O'Hare, D.; *Chem. Mater.* **2015**, *27*, 1495.
- Silveira, F.; Brambilla, R.; da Silveira, N.; Alves, M. C. M.; Stedile, F.; Pergher, S. C.; dos Santos, J. H. Z.; *J. Mater. Sci.* **2010**, *45*, 1760.
- Silveira, F.; Alves, M. C. M.; Stedile, F. C.; Pergher, S. B.; dos Santos, J. H. Z.; *J. Mol. Catal. A: Chem.* **2010**, *315*, 213.
- Ramachandra Rao, R.; Weckhuysen, B. M.; Schoonheydt, R. A.; *Chem. Commun.* **1999**, *5*, 445.
- Casas, E.; van Grieken, R.; Escola, J. M.; *Appl. Catal., A* **2012**, *437-438*, 44.
- Preishuber-Pflugl, P.; Brookhart, M.; *Macromolecules* **2002**, *35*, 6074.
- Brunauer, S.; Emmett, P. H.; Teller, E.; *J. Am. Chem. Soc.* **1938**, *60*, 309.
- Barrett, E. P.; Joyner, L. G.; Halenda, P. P.; *J. Am. Chem. Soc.* **1951**, *73*, 373.
- Meynen, V.; Cool, P.; Vansant, E. F.; *Microporous Mesoporous Mater.* **2009**, *125*, 170.
- Bagshaw, S. A.; Bruce, I. J.; *Microporous Mesoporous Mater.* **2008**, *109*, 199.
- Thommes, M.; Kaneko, K.; Neimark, A. V.; Olivier, J. P.; Rodriguez-Reinoso, F.; Rouquerol, J.; Sing, K. S. W.; *Pure Appl. Chem.* **2015**, *87*, 1051.
- Lee, J.-S.; Joo, S. H.; Ryoo, R.; *J. Am. Chem. Soc.* **2002**, *124*, 1156.
- Choi, Y.; Soares, J. B. P.; *Macromol. Chem. Phys.* **2009**, *210*, 1979.

Submitted: April 9, 2017

Published online: August 1, 2017

FAPERGS/CAPES has sponsored the publication of this article.